Charm and bottom hadroproduction with heavy-quark mass renormalized in the $\overline{\text{MS}}$ scheme

........,^{a} ....^{b}

^{a}*II. Institute for Theoretical Physics, Hamburg University*
  Luruper Chaussee 149, D–22761 Hamburg, Germany
^{b}*....*

  E-mail: x.y@desy.de

ABSTRACT: We present predictions for charm (bottom) production at hadron colliders making use of the $\overline{\text{MS}}$ renormalization scheme for the charm (bottom) mass, as an alternative to the widely used on-shell renormalization scheme. We compare these two possibilities, by showing single and double differential distributions including NLO QCD corrections complemented by the effects of phenomenological fragmentation functions, and total cross-sections at approximate NNLO accuracy. We briefly sketch possible interesting applications. This study is motivated by the observation that precise determinations of the value of the charm and bottom masses in the $\overline{\text{MS}}$ scheme are available, while the perturbative expansion for the conversion of the charm and bottom mass values from the $\overline{\text{MS}}$ scheme to the on-shell scheme is not converging, due to the smallness of the scales involved ($\sim$ very few GeV), not so far from the value of Λ_{QCD}, and to infrared renormalon singularities. In case of charm, a lack of convergence is already visible up to the 4-loop order, i.e. the accuracy at which the conversion to the pole mass value has been computed so far. We also provide public numerical routines, which can be used in the MCFM framework.

Contents

1 Introduction

Charm-anticharm and bottom-antibottom pair production are among the most frequent inelastic processes occurring in hadronic collisions at modern high-energy colliders, with cross-sections smaller than for the dijet case but well above those for the top-antitop case, as follows from the values of the masses of the various final-state partons, the available phase-space, and the structure of the Standard Model (SM) Lagrangian.

Collider experiments are able to detect the products of the hadronization / fragmentation of intermediate-mass quarks, i.e. heavy mesons and baryons, as well as the jet associated to them, i.e. b-jets and c-jets. B-hadrons and D-hadrons are reconstructed by their decay products, with decay vertices displaced with respect to the primary vertices. This operation requires good tracking, vertexing and particle identification capabilities. The measurements are indeed easier to perform in case of B-hadrons than for D-hadrons, because the proper lifetimes of the first ones are longer than those of the latter. In the reconstruction of the transverse momentum p_T of the decaying hadrons one has to take into account that at very low p_T, decay tracks can be affected by multiple scattering and that trigger efficiencies play a role in determining the minimum p_T of the decay products. On the other hand, the angle between the decay tracks become smaller as the p_T of the decaying object increases,

challenging the reconstruction process at large p_T, made even more difficult by the lower statistics. At large p_T, b-jet measurements, which not require a fully-exclusive reconstruction of the properties of the heavy decaying hadrons and do not distinguish between different B-hadron species, are still performed, made possible by the level of sophistication of b-jet tagging algorithms, that is rapidly increasing also thank to deep learning techniques. On the other hand, c-jet tagging is more difficult, but new promising methods and analyses adopting them are under development.

On the theory side, analytical formulas at the NLO accuracy for the cross-sections for the hadroproduction of massive quark pairs, as well as for one-massive-quark inclusive production, are known since many years. The resummation of logarithms of (p_T^2/m^2), relevant when the transverse momentum of the heavy-quark p_T is much larger than its mass m, has been performed up to the next-to-leading-logarithmic (NLL) accuracy. The resummation of Sudakov logarithms related to radiation with $p_T \to 0$, as well as the one of threshold logarithms and high-energy logarithms, have also been worked out (up to various degrees of accuracy) and presented in a number of papers. The transition from quarks to hadrons is described either by Fragmentation Functions, or by matching NLO matrix-elements to parton shower and hadronization approaches. Differential cross-sections are known at NNLO accuracy only for top-antitop hadroproduction, eventually complemented by the resummation of threshold logarithms at the netx-to-NLL (NNLL) accuracy, but not yet for the charm and bottom cases. In case of the latter, however, approximate total NNLO cross-sections are also available.

One of the inputs of all aferomentioned calculations are the values of the heavy-quark masses. The SM is not able, by itself, to predict the values of the quark masses, which are thus fundamental parameters in this framework. In general, different renormalization schemes can be used for relating the bare masses to the renormalized ones, and predictions for physical observables on the basis of a truncated pQCD series, relying on renormalized quantities, are scheme dependent. It follows that even the perturbative convergence can vary from scheme to scheme.

In this paper we describe the use of the $\overline{\text{MS}}$ scheme, as an alternative to the most widely used on-shell scheme, for the renormalization of the charm (bottom) masses in charm (bottom) production at hadron colliders. We investigate the perturbative convergence in both schemes, by providing comparisons between physical quantities calculated at various levels of accuracy, and we sketch interesting applications within and beyond collider physics.

The implementation of the calculation of single and double differential distributions, including NLO QCD corrections and using the $\overline{\text{MS}}$ scheme for renormalizing the charm (bottom) mass is described in Section 2. The details of the corresponding numerical routines released as an addendum to this paper are collected in the Appendix. Predictions obtained using this implementation are presented in Section **??**, whereas predictions for total cross-sections, up to approximate NNLO accuracy, are

presented in Section 4, together with considerations on the convergence of the perturbative expansion in the strong coupling constant. Examples of possible applications are briefly discussed in Section 5. Finally, our conclusions are summarized in Section 6

2 Implementation

1)...formulas....

In this work light quarks are assumed to be massless. On the other hand, for the heavy-quark masses, different renormalization schemes can be adopted. In the following we focus on the cases of the $\overline{\text{MS}}$ and on-shell schemes and we explicitly recall the conversion relation between the values of the renormalized masses in these two schemes. Other mass choices would also be possible, e.g. the potential subtractive mass was suggested as a possibility to produce an improved perturbative convergence for heavy quark production near threshold (i.e. at energies slightly above $2m_Q$) in Ref. [1] and the 1S mass have been introduced in Ref. [2] as a way of stabilizing the position of the peak of the vector-current-induced total cross section of $t\bar{t}$ production in e^+e^- collisions, as a function of $\sqrt{s}$, for $\sqrt{s} \sim 2\ m_t$. Limited to the case of top quarks, the top quark jet mass [3], was introduced in the framework of Soft Collinear Effective Theory.

In the $\overline{\text{MS}}$ scheme, the renormalized mass of the heavy-quark vary with the renormalization scale μ_R. The evolution follows the renormalization group equation (RGE)

$$\mu_R^2 \frac{dm(\mu_R)}{d\mu_R^2} = -\gamma(\alpha_S(\mu_R))m(\mu_R) \tag{2.1}$$

where $\gamma(\alpha_S(\mu_R)) \equiv \sum_{r=1}^{\infty} \gamma_r(\alpha_S(\mu_R)/\pi)^r$ is the anomalous dimension, known up to four-loop order in perturbation theory, depending on the coupling constant α_S, also renormalized in the same scheme. Explicit formulas for the γ_1, γ_2, γ_3 and γ_4 coefficients, depending on the number of active light quark flavours at the scale μ_R, are given in the literature.

Precise determinations of the $\overline{\text{MS}}$ masses of heavy-quarks are available from a number of studies.

In the on-shell scheme, the renormalized mass coincides with the pole in the Fourier transform of the Feynman propagator of the renormalized quark field and is thus the same at all scales. Considering its infrared finiteness to all orders in perturbation theory, this is the natural mass parameter for the description of heavy-quark systems at scales governed by the mass of the heavy quark. However, this definition is based on the concept of quarks as asymptotic states, which can rise a number of issues. One of them is that the pole mass is not an observable, because of confinement.

The on-shell (also called pole) mass M can be obtained from the $\overline{\text{MS}}$ running mass m at a renormalization scale μ_R, in terms of an perturbative expansion in the strong coupling constant α_S:

$$M = m(\mu_R)\left(1 + c_1\left(\frac{\alpha_S}{\pi}\right) + c_2\left(\frac{\alpha_S}{\pi}\right)^2 + c_3\left(\frac{\alpha_S}{\pi}\right)^3 + \mathcal{O}(\alpha_S^3)\right) \tag{2.2}$$

with the coefficients c_1, c_2, c_3 given by

$$c_1 = C_F\left(1 + \frac{3}{4}L\right) \tag{2.3}$$

$$c_2 = ... \tag{2.4}$$

$$c_3 = ... \tag{2.5}$$

where $C_F = 4/3$ is one of the SU(3) color factors, $L \equiv \ln(\mu_R^2/m(\mu_R)^2)$, and α_S is evaluated at the $m(\mu_R)$ scale and renormalized in the $\overline{\text{MS}}$ scheme in the theory with a number of active flavours equal to $n_f = n_{lf} + 1$ at and above the heavy-quark threshold scale, assumed to be equal to its mass. The number of light flavours is $n_{lf} = 3$ (4) for charm (bottom) production, respectively.

Considering the particular case of $m(m)$, i.e. the $\overline{\text{MS}}$ mass renormalized at the scale $\mu_R = m(\mu_R)$, $m(m) \equiv m(\mu_R = m(\mu_R))$, the logarithmic terms L cancel and, evaluating eq. 2.2 numerically, one gets [4]:

$$M = m(m)\left(1 + 1.333\left(\frac{\alpha_S}{\pi}\right) + (13.44 - 1.041n_{lf})\left(\frac{\alpha_S}{\pi}\right)^2 + \right.$$
$$\left. + \left(190.595 - 27.0n_{lf} + 0.653n_{lf}^2\right)\left(\frac{\alpha_S}{\pi}\right)^3 + \mathcal{O}(\alpha_S^3)\right) \tag{2.6}$$

On the other hand, inverting this relation and making a Taylor expansion, one gets $m(m)$ as a function of the pole mass

$$m(m) = M\left(1 - 1.333\left(\frac{\alpha_S}{\pi}\right) + (-11.67 + 1.041n_{lf})\left(\frac{\alpha_S}{\pi}\right)^2 + \right.$$
$$\left. + \left(-170.0 + 24.8n_{lf} - 0.653n_{lf}^2\right)\left(\frac{\alpha_S}{\pi}\right)^3 + \mathcal{O}(\alpha_S^3)\right) \tag{2.7}$$

When using eq. 2.7, we evaluate α_S in the $\overline{\text{MS}}$ scheme in the theory with n_f active flavours at the scale $\mu_R = M$.

While α_S in eq. 2.2, 2.6, 2.7 is renormalized in the $\overline{\text{MS}}$ scheme, the matrix-elements, as well as the parton distribution functions (PDF) and the associated α_S evolution used in the fixed-order massive calculations presented in this paper are all defined in the decoupling scheme, with a fixed number of light flavours $n_{lf} = 3$ for charm production and $n_{lf} = 4$ for bottom production at all scales. Using the decoupling relations, it is possible to express the PDFs, α_S and the partonic cross-sections in the $\overline{\text{MS}}$ scheme in terms of those in the decoupling scheme, once fixed a

scale μ. Alternatively, it is also possible to re-express eq. 2.6 in terms of α_S in the decoupling scheme, obtaining

$$M = ... \tag{2.8}$$

In practice, although terms for the expansion in eq. 2.2, 2.6, 2.7 are known up to 4-loops [5], we truncate it at two-loops (order α_S^2) for computing the NNLO cross-sections and at one-loops (order α_S) for computing NLO cross-sections, respectively.

In this work, the α_S evolution as a function of μ_R and the corresponding α_S values entering in eq. 2.2, 2.6 and 2.7 and other parts of the fixed-order computation are evaluated retaining three-loops for producing NNLO cross-sections and two-loops for producing the NLO ones, respectively, although other choices would indeed be possible, as follows from the fact that solving RGE equations, relating running quantities at different μ_R scales, is an all-loop operation.

The presence of infrared renormalon singularities in the relation of conversion from the pole mass to the $\overline{\text{MS}}$ mass manifests in practice as factorially growing terms in the expansion in eq. 2.2, that does not converge. Treating the series as an asymptotic expansion, the ambiguity in its resummation, affecting the value of the pole mass, is of the order of $\mathcal{O}(\Lambda_{QCD})$.

While the pole mass is plagued by the renormalon ambiguity uncertainty, the short-distance mass definitions are renormalon-free.

2) may be add a plot with comparison between m(μ_R) as a function of μ_R, and M (constant) as a function of μ_R ?

3)...MNR and MCFM....

4) some example of cross-check between the two codes (MCFM, MNR) and a pair of figures showing they give the same results

3 Predictions for differential cross-sections

1) Comparisons between LO and NLO for a number of differential distributions (i.e. all possible kinds of $d\sigma/dX$ implemented in the MNR/MCFM program, with no cuts at all, and with different sets of cuts, for both charm and bottom. Also add the case where $X = m_{Q\bar{Q}}$ considering that this is interesting for some ongoing experimental analyses (see CMS) for extracting the running mass of the top quark (and a similar

methodology may be can be extended even to the extraction of charm and bottom masses ?). The reason of studying also LO, even if, in case of charm, I agree it has gigantic uncertainty bands, is that we want to have idea of the convergence of the cross-sections when using running mass with respect to the case of using pole masses. To do this, we would ideally better compare NLO and NNLO, however, considering that we do not have any NNLO differential distributions, the only thing we can do for now for studying convergence of differential distribution is comparing NLO with LO. I think one could put in the paper some differential K-factor, making ratios of differential distributions at NLO and LO, to see if K-factors using running masses are a bit smaller than those using the pole masses or not and give some quantitative number to the people. One could compare the perturbative convergence in case of charm and in case of bottom. The LO predictions One could put just in a few plots (e.g. when drawing distributions without cuts or with purely theoretical cuts), not necessarily in the plots with the experimental cuts and explicit comparison with experimental data. In fact, I am thinking to distributions of charm and bottom quarks, not even D-mesons or B-mesons.

2) Check if, using stronger systems of cuts, the implementation in the running mass scheme behaves better than the other or if the behaviour of scale uncertainties remains similar to what we have already observed for the LHCb cuts (i.e. no strong changes).

Among other things, I would look, maybe, at large p_T, again for case of charm and bottom quarks (and not the mesons). I have not a specific suggestion for a system of cuts, but, in general, the more exclusive the system of cuts are, the most I would expect distributions to change between two different implementations.

3) Possible double differential distributions $\frac{d^2\sigma}{dp_T dy}$, $\frac{d^2\sigma}{dm_{Q\bar{Q}} dy}$ and importance for comparison with experimental measurements. One can make reference to recent experimental studies of top quarks by CMS.

4) One can try to use different scales. One could e.g. also try to use Czakon/Mitov suggested scales for top, and show how they work (or do not work) for bottom and charm.

———————————————————————————————

We compare the pole masses, m^{pole}, with the $\overline{\mathrm{MS}}$ masses, $m(m)$, and MSR masses, $m^{\mathrm{MSR}}(R)$, for charm, bottom and top quarks in Table 1.[1] The relations

———————————

[1] For the top quark masses, such comparison has been already presented in [6].

MSR(1)	MSR(3)	MSR(9)	$m(m)$	$m^{\mathrm{pl}}_{\mathrm{1lp}}$	$m^{\mathrm{pl}}_{\mathrm{2lp}}$	$m^{\mathrm{pl}}_{\mathrm{3lp}}$	$m^{\mathrm{pl}}_{\mathrm{1lp}}$	$m^{\mathrm{pl}}_{\mathrm{2lp}}$	$m^{\mathrm{pl}}_{\mathrm{3lp}}$
top quark									
171.9	171.6	170.9	162.0	169.5	171.1	171.6	171.9	172.0	172.1
172.9	172.6	172.0	163.0	170.5	172.2	172.7	172.9	173.1	173.2
174.0	173.7	173.0	164.0	171.6	173.2	173.7	174.0	174.1	174.2
bottom quark									
4.73	4.31	3.61	4.15	4.60	4.83	4.99	4.68	4.89	5.07
4.76	4.35	3.64	4.18	4.63	4.86	5.03	4.71	4.92	5.10
4.80	4.38	3.68	4.21	4.66	4.89	5.06	4.75	4.96	5.13
charm quark									
1.33	0.91	0.21	1.25	1.50	1.72	2.02	1.28	1.49	1.67
1.37	0.95	0.25	1.28	1.53	1.75	2.05	1.32	1.53	1.70
1.40	0.99	0.28	1.31	1.56	1.78	2.07	1.36	1.57	1.74

Table 1. Numerical values for heavy-quark MSR, $\overline{\mathrm{MS}}$ and pole masses. Columns 1–3 and 4 show the MSR masses at different scales and the $\overline{\mathrm{MS}}$ mass, respectively. These values are converted at $O(\alpha_s^3)$ for $\alpha_s(M_Z)^{n_f=5} = 0.118$ ($\alpha_s(M_Z)^{n_f=3} = 0.106$) for top (charm, bottom) quarks. Columns 5–7 show the 1, 2 and 3 loop pole masses converted from the $\overline{\mathrm{MS}}$ mass. Columns 8–10 show the 1, 2 and 3 loop pole masses converted from the MSR mass at $R = 3$ GeV. All values are given in GeV.

between the different masses are [7–10]:

$$
\begin{aligned}
m^{\mathrm{pole}} &= m(m)[1 + \Sigma_{n=1}^{\infty} d_n(\alpha_s/\pi)^n], \\
m^{\mathrm{pole}} &= m^{\mathrm{MSR}}(R) + R\Sigma_{n=1}^{\infty} a_n[\alpha_s(R)/(4\pi)]^n.
\end{aligned}
\tag{3.1}
$$

The numerical coefficients d_n and a_n can be found in Refs. [7–9] and Ref. [10], respectively. In the calculations, we use 3 light flavours when working with the charm and bottom quarks, and 5 light flavours when working with the top quark. The running of the $\overline{\mathrm{MS}}$ heavy-quark masses is shown in Fig. 1 (left). It is calculated at one loop using the RunDec program [11]. The dependence of the MSR heavy-quark masses on R at one loop is shown in Fig. 1 (right). It is calculated according to the solution of the RGE equation [10]:

$$
m^{\mathrm{MSR}}(R) = m^{\mathrm{MSR}}(R_0) - \int_{\ln R_0}^{\ln R_1} R\gamma_R[\alpha_s(R)]\mathrm{d}\ln R.
\tag{3.2}
$$

The function $\gamma_R(x)$ can be found in Ref. [10]. It is expanded to lowest non-vanishing order of α_s.

We computed double-differential cross sections as functions of p_T and y of the heavy quark (Q) and single-differential cross sections as a function of the invariant mass of the heavy quark pair in the pole, $\overline{\mathrm{MS}}$ and MSR mass schemes at NLO $O(\alpha_s^3)$ using the MCFM [12, 13] with modifications [14] and xFitter [15] frameworks. In
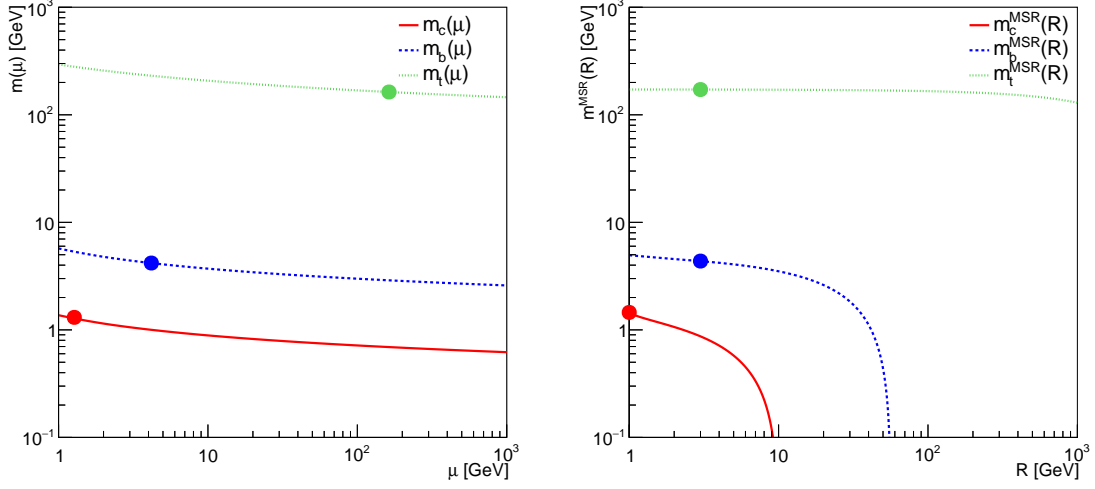
Figure 1. (left) The running $\overline{\text{MS}}$ heavy-quark masses. (right) The dependence of the MSR heavy-quark masses on R. The values of μ and R which are used in the calculations are marked with filled dots.

both cases, the original NLO calculations are done in the pole mass scheme [16]. These cross sections are converted to the $\overline{\text{MS}}$ or MSR mass schemes by expanding in α_s, analogous to Ref. [14]:

$$
\begin{aligned}
\sigma(m(m)) &= \sigma(m^{\text{pole}})\Big|_{m^{\text{pole}}=m(m)} + (m(m) - m^{\text{pole}})\left(\frac{\text{d}\sigma^0}{\text{d}m}\right)\Big|_{m^{\text{pole}}=m(m)}, \\
\sigma(m^{\text{MSR}}) &= \sigma(m^{\text{pole}})\Big|_{m^{\text{pole}}=m^{\text{MSR}}} + (m^{\text{MSR}} - m^{\text{pole}})\left(\frac{\text{d}\sigma^0}{\text{d}m}\right)\Big|_{m^{\text{pole}}=m^{\text{MSR}}}.
\end{aligned}
\tag{3.3}
$$

Here σ^0 is the Born contribution to the cross section, and the differences $m(m) - m^{\text{pole}}$ and $m^{\text{MSR}} - m^{\text{pole}}$ are calculated to lowest non-vanishing order in α_s, such that all terms of $O(\alpha_s^4)$ are dropped in Eq. 3.3, as appropriate for a NLO calculation at $O(\alpha_s^3)$. The modified MCFM program [14] is capable to convert the pole mass NLO calculations into the $\overline{\text{MS}}$ mass scheme for single-differential cross sections as functions of p_T of the heavy quark, y of the heavy quark or invariant mass M of the heavy-quark pair. The derivative of the Born contribution is calculated semi-analytically in MCFM [14]. xFitter converts the pole mass NLO cross sections into the the $\overline{\text{MS}}$ or MNR mass schemes for fully differential, but only one-particle inclusive, distributions, i.e. it is capable to compute the double differential cross section as a function of p_T and y of the heavy quark, but not as a function of the invariant mass of the heavy-quark pair. The derivative in Eq. 3.3 is computed numerically in xFitter. The differential cross sections in different schemes which can be computed by MCFM and xFitter are summarised in Table 2. For cross sections in the pole mass scheme and for cross sections as a function of p_T or y in the $\overline{\text{MS}}$ mass schemes, the MCFM and

Cross section	pole mass scheme	$\overline{\text{MS}}$ mass scheme	MSR mass scheme
$\mathrm{d}\sigma/\mathrm{d}p_T$	M,X	M,X	X
$\mathrm{d}\sigma/\mathrm{d}y$	M,X	M,X	X
$\mathrm{d}\sigma/\mathrm{d}M$	M,X	M	–
$\mathrm{d}^2\sigma/\mathrm{d}p_T\mathrm{d}y$	M,X	X	X

Table 2. Summary of the capability of the MCFM (M) and xFitter (X) frameworks to compute differential cross sections for heavy-quark hadroproduction in different mass schemes.

xFitter calculations agree within percent accuracy [cite thesis of Lucas Kemmler].[2]

In the calculations, we use the $\overline{\text{MS}}$ charm and bottom quark masses $m_c(m_c) = 1.28$ GeV and $m_b(m_b) = 4.18$ GeV [17], and the $\overline{\text{MS}}$ top quark mass $m_t(m_t) = 163$ GeV [10, 18]. For the pole and MSR masses, the corresponding values from Table 1 are used which are obtained by converting the $\overline{\text{MS}}$ masses into the MSR or pole masses. For MSR masses, the value of R is chosen $R = 3$ GeV for the bottom and top quarks, and $R = 1$ GeV for the charm quark (to avoid using too small value of m_c^{MSR} at $R = 3$ GeV). For the pole masses, the values obtained by converting from the $\overline{\text{MS}}$ mass at one loop are chosen (column 5 in Table 1). The factorisation and renormalisation scales are set to $\mu_r = \mu_f = \sqrt{4m^2 + p_T(Q)^2}$. The proton is described by the ABMP16 NLO PDF set [19]. To estimate the theoretical uncertainties, the factorisation and renormalisation scales are varied by a factor of two up and down, both simultaneously and independently for μ_r and μ_f. All calculations are provided for pp collisions at the LHC at a centre-of-mass energy of $\sqrt{s} = 7$ TeV.

In Fig. 2 the NLO differential cross sections with their scale uncertainties as a function of p_T in intervals of y of the charm quark in the pole, $\overline{\text{MS}}$ and MSR mass schemes calculated using xFitter are shown. When using the $\overline{\text{MS}}$ or MSR mass scheme instead of the pole mass scheme, the changes of the cross sections amount to 0–35%, which are however small compared to the NLO scale uncertainties. The latter amount to a factor of 2 in the bulk of the phase space, decreasing slightly towards large p_T values. The scale uncertainties are very similar in all mass schemes.
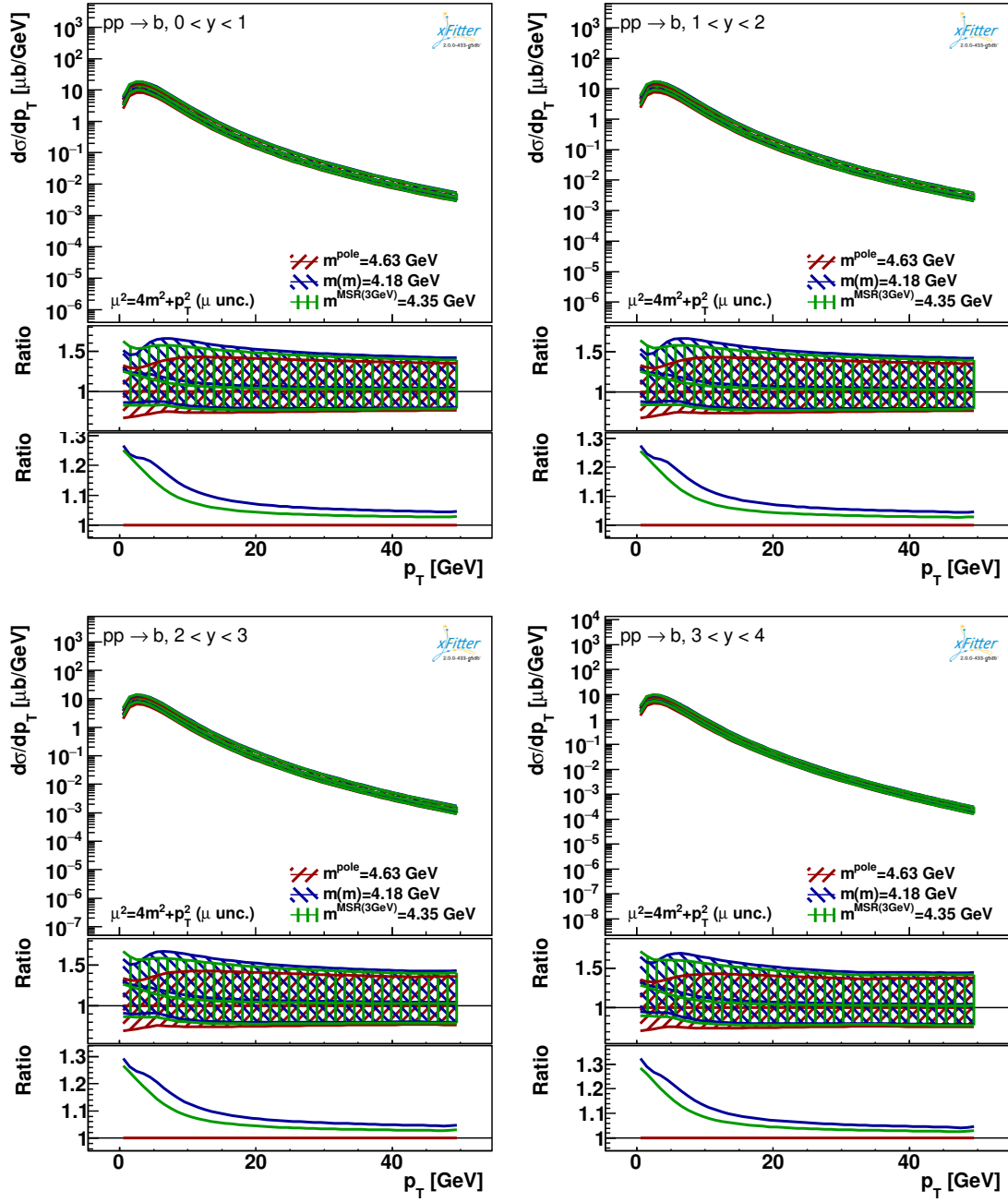
In Fig. 3 the same comparison of NLO differential cross sections in the various mass schemes is presented for bottom quark production. In this case, the impact of converting the pole mass calculations into the $\overline{\text{MS}}$ or MSR schemes is 0–25% and is

---

[2]We note that while the MCFM and xFitter results (the latter are based on the MNR calculations [16]) calculated using $\mu_r = \mu_f$ agree within about 1% for all heavy quarks, those charm production cross sections which are calculated using $\mu_r \neq \mu_f$ differ by about 10% in some phase-space regions, in particular at low p_T [cite thesis of Lucas Kemmler]. However, this level of agreement is satisfactory given that the NLO scale uncertainties are still larger by one order of magnitude.
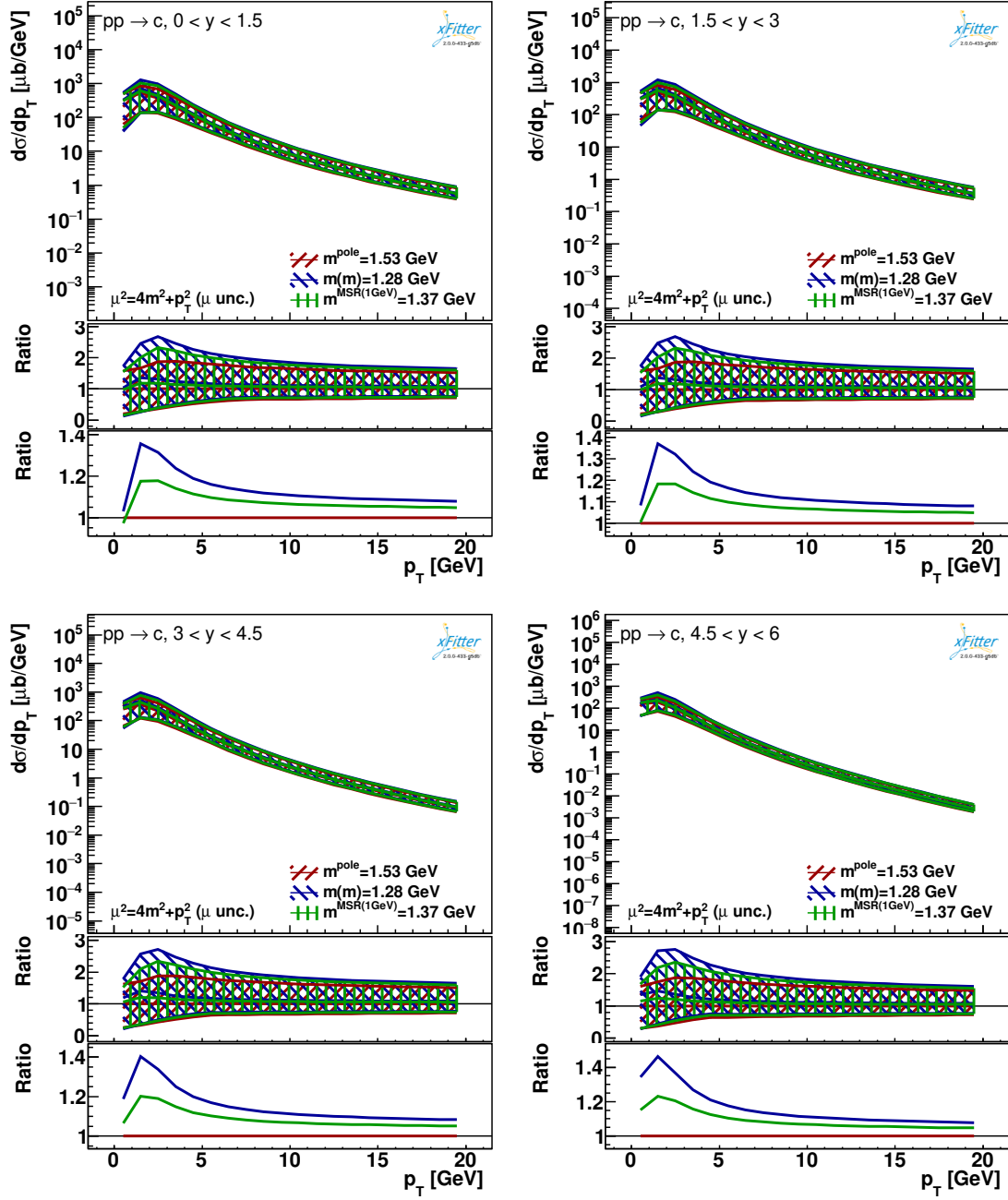
Figure 2. The NLO differential cross sections for charm production with their scale uncertainties as a function of p_T in intervals of y of the c quark in the pole $\overline{\text{MS}}$ and MSR mass schemes at the LHC ($\sqrt{s} = 7$ TeV). The bottom panels display the theoretical predictions normalized to the values obtained in the pole mass scheme.

still small compared to the NLO scale uncertainties of the order of 50%. The scale uncertainties are similar in the pole and MSR mass schemes, while in the $\overline{\text{MS}}$ mass scheme they are slightly smaller at low p_T.

Figure 3. The NLO differential cross sections for bottom production with their scale uncertainties as a function of p_T in intervals of y of the b quark in the pole, $\overline{\text{MS}}$ and MSR mass schemes at the LHC ($\sqrt{s} = 7$ TeV). The bottom panels display the theoretical predictions normalized to the values obtained in the pole mass scheme.

Finally, in Fig. 4 the same comparison is presented for top quark production. In this case, the impact of converting the pole mass calculations into the $\overline{\text{MS}}$ mass scheme is about 20% at low p_T which is no longer small compared to the NLO scale

uncertainties. It decreases towards higher p_T values. When converting the cross sections to the MSR mass scheme, the impact is below $< 10\%$ and is within the NLO scale uncertainties. The scale uncertainties in the $\overline{\text{MS}}$ mass scheme are slightly smaller than in the pole mass scheme, as was already reported in Ref. [14], while the scale uncertainties in the MSR and pole mass schemes are very similar.

Furthermore, in Figs. 5 and 6 we compare the theoretical uncertainties of the NLO calculations which arise due to quark mass variations of $m_c(m_c) = 1.28 \pm 0.03$ GeV and $m_b(m_b) = 4.18 \pm 0.03$ GeV [17] in the $\overline{\text{MS}}$ mass scheme, and $m_c^{\text{pole}} = 1.53 \pm 0.25$ GeV, $m_b^{\text{pole}} = 4.63 \pm 0.25$ GeV in the pole mass scheme. The latter variations reflect the fact that the pole mass is affected by an intrinsic uncertainty of the order of Λ_{QCD}. Therefore, calculations in the $\overline{\text{MS}}$ or MSR mass schemes afford substantially smaller uncertainties (in particular at low p_T) due to quark mass variations.

In Fig. 7 the single-differential cross sections as a function of the invariant mass of the heavy-quark pair in the pole and $\overline{\text{MS}}$ mass scheme calculated using MCFM are shown (no calculation in the MSR scheme is available for this distribution). The impact of changing the pole to $\overline{\text{MS}}$ mass scheme is largest at lowest values of M close to the production threshold. This is because the lower values of the $\overline{\text{MS}}$ masses lead to lower threshold values and thus to a larger cross section near it. *SZ: is it really reasonable? In the $\overline{\text{MS}}$ mass scheme, should not one keep using *on-shell* mass as the kinematic mass of heavy quark (i.e. its four-momentum squared), and thus keeping the threshold at $2m^{pole}$?* Furthermore, as was noticed in Ref. [14], very close to the production threshold the derivative term in Eq. 3.3 becomes large and cause the invariant mass spectrum to dip below zero for values very close to the threshold, indicating the breakdown of fixed-order perturbation theory.
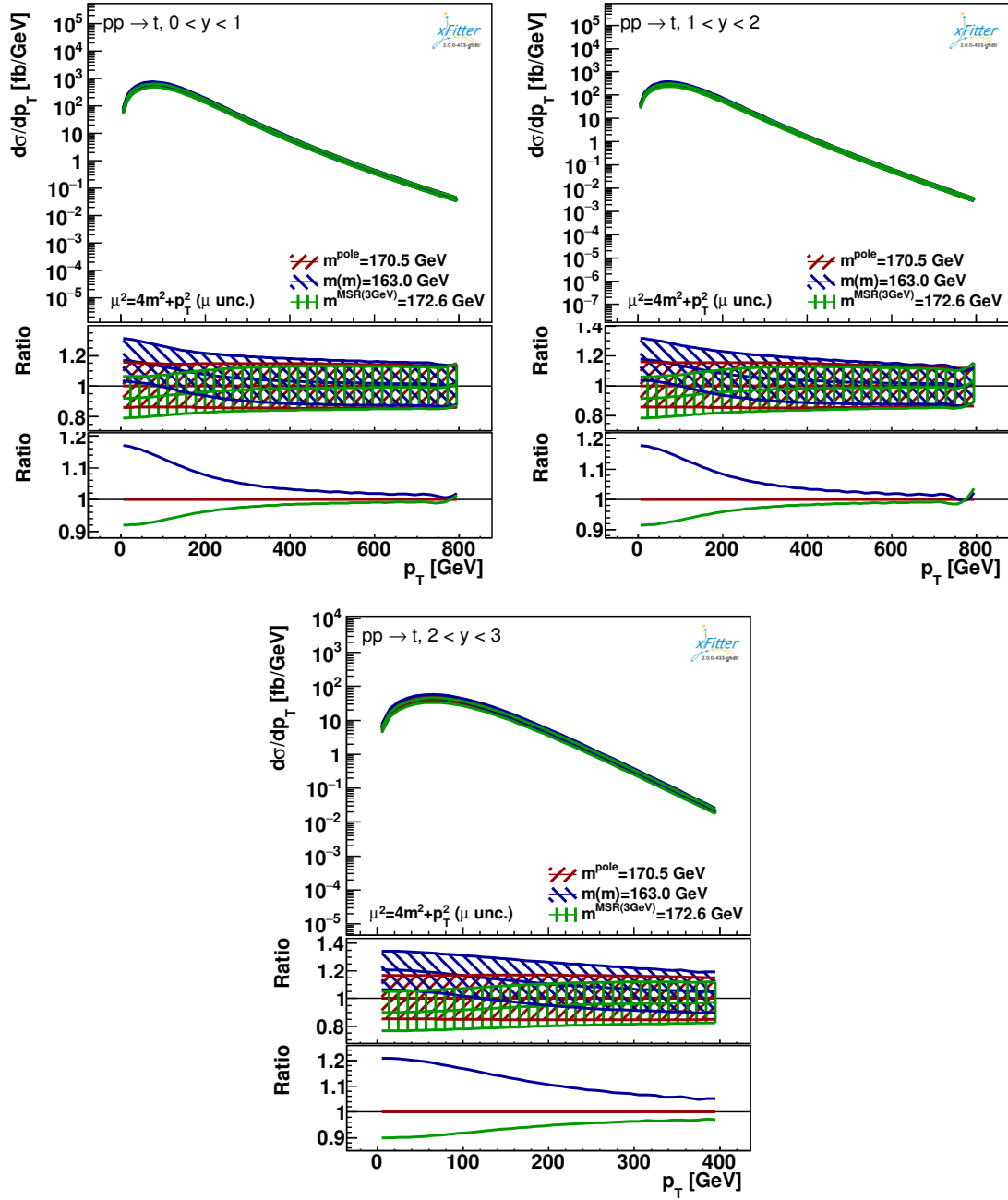
4 Predictions for total cross-sections

1) Comparison of LO, NLO, NNLO cross-sections using Hathor with on-shell vs $\overline{\text{MS}}$ scheme. Even if we have already presented some of these comparisons in our old paper, one could make further updated ones, to see the convergence of the perturbative series, and comparisons using the most modern PDFs.

5 Possible applications

5.1 NLO PDF fits with differential charm hadroproduction cross sections

One of the possible applications of the calculations for heavy-quark hadroproduction with the $\overline{\text{MS}}$ mass definition could be PDF fits which use heavy-flavour measurements
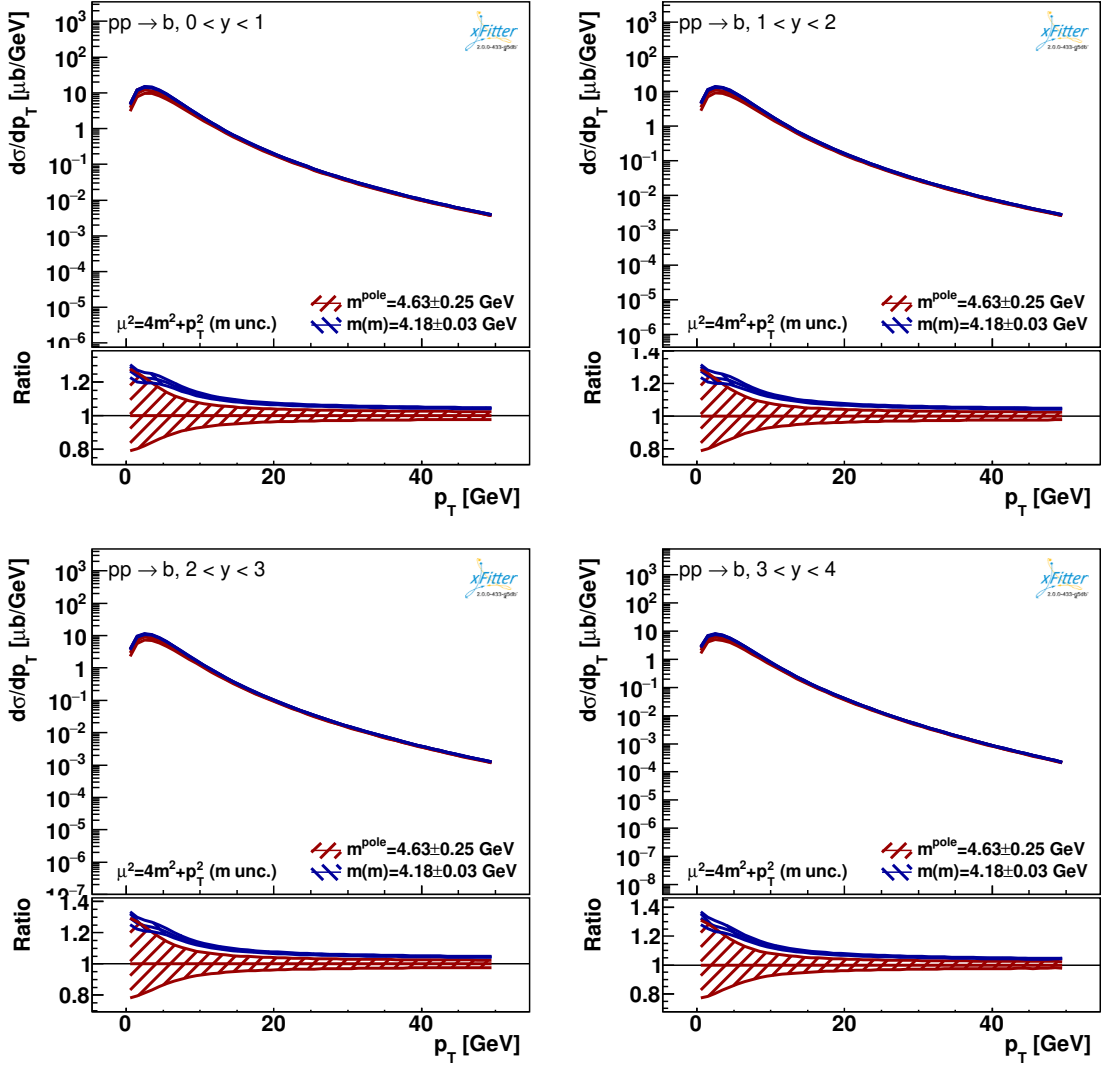
Figure 4. The NLO differential cross sections for top production with their scale uncertainties as a function of p_T in intervals of y of the t quark in the pole, $\overline{\text{MS}}$ and MSR mass schemes at the LHC ($\sqrt{s} = 7$ TeV). The bottom panels display the theoretical predictions normalized to the values obtained in the pole mass scheme.

from the LHC to constrain the gluon distribution at low values of x [20–22]. Because of the large scale dependence of the NLO calculations for charm hadroproduction, in such fits it seems feasible to include only ratios of cross sections, which are constructed
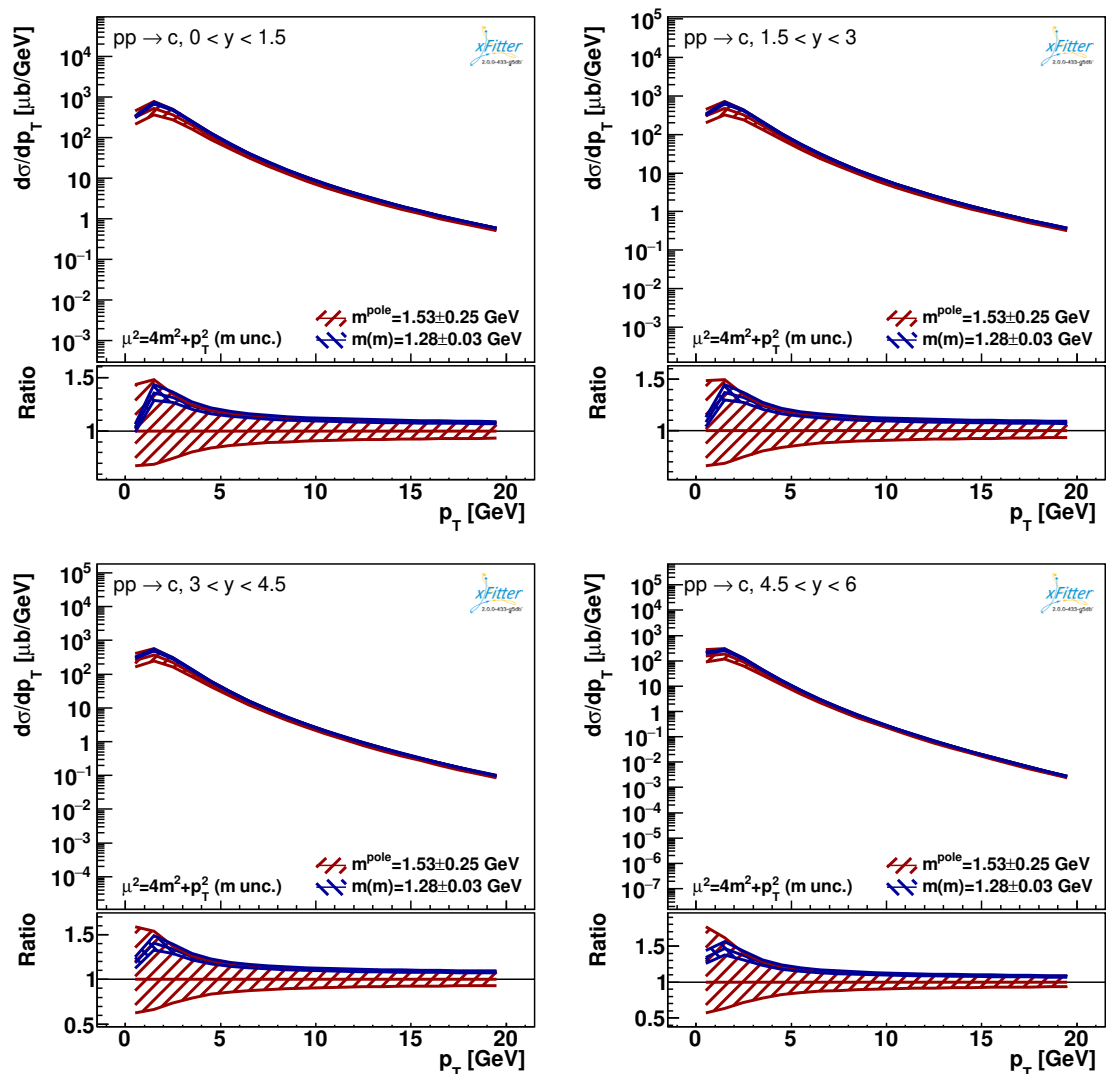
Figure 5. The NLO differential cross sections for charm production with their uncertainties due to mass variations as a function of p_T in intervals of y of the c quark in the pole and $\overline{\text{MS}}$ mass schemes at the LHC ($\sqrt{s} = 7$ TeV). The bottom panels display the theoretical predictions normalized to the values obtained in the pole mass scheme.

using measurements at different values of rapidity and/or transverse momentum, or at different centre-of-mass energies. As an example, in the PROSA analysis [20] ratios of charm and bottom hadron production cross sections [23, 24] as a function of rapidity to the cross section in the $3 < y < 3.5$ interval for each p_T bin were used, together with the inclusive DIS data from HERA [25–27]. These ratios afforded a reduced scale dependence, but at the same time they have reduced sensitivity to the heavy-quark mass. We repeat the PROSA analysis using the $\overline{\text{MS}}$ heavy-quark masses both in the calculations of the DIS structure functions and charm and bottom hadroproduction cross sections, while all other settings are as in Ref. [20], and observe

– 14 –

Figure 6. The NLO differential cross section for bottom production with their uncertainties due to mass variations as a function of p_T in intervals of y of the b quark in the pole and $\overline{\text{MS}}$ mass schemes at the LHC ($\sqrt{s} = 7$ TeV). The bottom panels display the theoretical predictions normalized to the values obtained in the pole mass scheme.

only small impact on χ^2 and fitted PDFs, which are well within the uncertainties. Even these small differences are driven mainly by the change in the predictions for the HERA data, because the LHCb data in the format of the normalised cross sections do not provide notable sensitivity neither to the heavy-quark mass scheme, not to the value of the heavy-quark mass. As a result, the fitted $\overline{\text{MS}}$ and pole masses come out:

$$m_c(m_c) = 1.17 \pm 0.05 \text{ GeV}, \qquad m_c^{\text{pole}} = 1.26 \pm 0.06 \text{ GeV},$$
$$m_b(m_b) = 3.98 \pm 0.14 \text{ GeV}, \qquad m_b^{\text{pole}} = 4.19 \pm 0.14 \text{ GeV}. \tag{5.1}$$
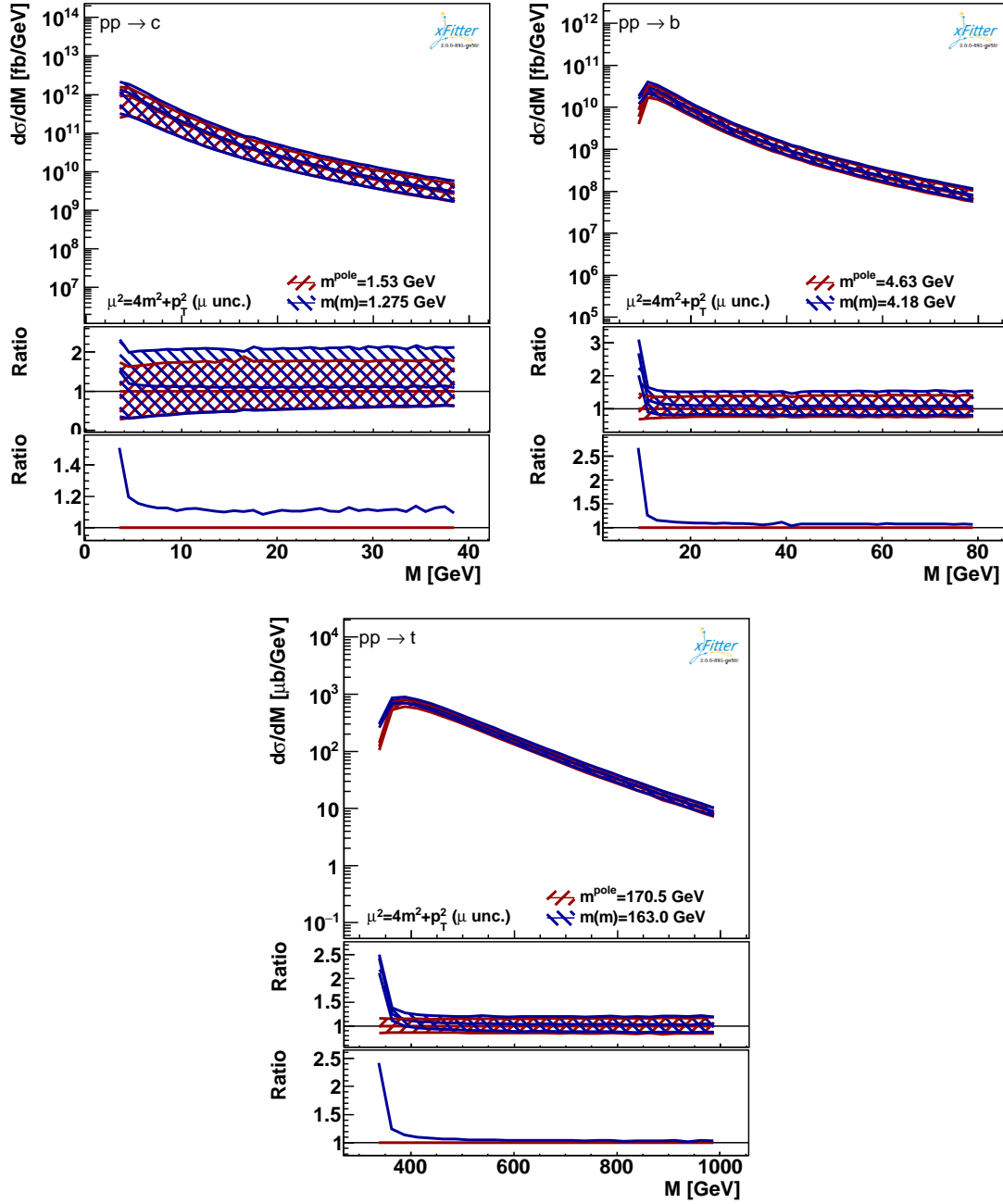
Figure 7. *SZ: These plots will be updated with larger statistics to smooth fluctuations.* The NLO differential cross sections for charm (top left), bottom (top right) and top (bottom) hadroproduction with their scale uncertainties as a function of the invariant mass of the heavy-quark pair in the pole and $\overline{\text{MS}}$ mass schemes at the LHC ($\sqrt{s} = 7$ TeV). The bottom panels display the theoretical predictions normalized to the values obtained in the pole mass scheme.

The quoted uncertainties are fit uncertainties only. The $\overline{\text{MS}}$ masses are compatible with the results obtained in Refs. [26–29] where the HERA data alone were analysed

to determine the heavy-quark $\overline{\text{MS}}$ masses. They are also in a better agreement with the world average values [17], than the pole masses, indicating that the latter carry a significant intrinsic theoretical uncertainty.

5.2 Extraction of $m_t(m_t)$ and $m_t^{\textbf{MSR}}$ from differential $t\bar{t}$ cross sections at NLO

The mass of the top quark can be extracted using measurements of total or differential $t\bar{t}$ production cross sections. As an example, we use the recent CMS measurement [30] of normalised triple-differential $t\bar{t}$ cross sections as a function of invariant mass and rapidity of the $t\bar{t}$ pair, and the number of additional jets, to extract the values of $m_t(m_t)$ and m_t^{MSR} in a simultaneous fit with α_s and PDFs, and compare the results with the ones obtained in the CMS analysis [30]. These observables provide decent sensitivity to the top quark mass, α_s and PDFs, i.e. to the complete set of input theoretical parameters of fixed-order calculations for stable top quark pair production. In particular, the distributions of $t\bar{t}$ invariant mass and additional jet multiplicity are sensitive to the top quark mass through threshold and cone effects [31].

The QCD analysis setup follows the original CMS analysis [30], and the detailed description of the fitting procedure can be found in Section 10 of Ref. [30], while below only the main settings are summarised. The QCD analysis is done using the xFitter framework [15]. Theoretical predictions for the $t\bar{t}$ data are obtained at NLO in the pole mass scheme using the MadGraph5_aMC@NLO program [32], interfaced with aMCfast [33] and ApplGrid [34] to store the calculated cross sections bin-by-bin in the format which is suitable for PDF fits with xFitter. The dependence of the theoretical predictions on the top quark mass is taken into account by generating several sets of predictions with different values of this parameter and smoothly interpolating them in the fit. The HERA DIS data [35] are included in the fit to provide constraints on the valence and sea quark distributions and probe the gluon distribution and α_s through scaling violations, while the CMS $t\bar{t}$ provide direct constraints on the gluon PDF and α_s, as well as on the top quark mass as discussed in Ref. [30]. Further details can be found in Ref. [30].

In our analysis, we convert the NLO calculations for $t\bar{t}$ production cross sections from the pole mass scheme into the $\overline{\text{MS}}$ or MSR mass schemes according to Eq. 3.3. Because the calculated cross sections are stored in ApplGrid tables as bin integrated cross sections, it is not possible to use a dynamic scale $\mu_r = \mu_f = H'$ defined as one half of the sum of transverse masses of the final-state partons (see Section 9 of Ref. [30]), since H' is not constant within the bin. Instead, we use a static scale $\mu_r = \mu_f = m_t$, and we also repeat the extraction of the pole mass with this scale choice. As the analysis of triple-differential $t\bar{t}$ cross sections requires NLO predictions for not only inclusive $t\bar{t}$ production of $O(\alpha_s^3)$, but also for inclusive $t\bar{t}+1$ jet production of $O(\alpha_s^4)$, MadGraph5_aMC@NLO is the only public code we know which provides such calculations and is interfaced to ApplGrid.

The fit results obtained using different mass schemes are given in Table 3. The values of χ^2 characterise fit quality. These values are very similar in all fit variants and illustrate good description of the $t\bar{t}$ data. To estimate uncertainties, we follow the procedure from Ref. [30] and determine fit, model, parametrisation and scale variation uncertainties. As in the CMS analysis, the scales are varied coherently in all bins of the measured cross sections. In the pole mass scheme, switching from the dynamic scale to the static scale changes the extracted pole mass by about 0.5 GeV, but further enlarges the scale uncertainties substantially. Therefore, the larger scale uncertainties obtained in this analysis using the $\overline{\text{MS}}$ or MSR mass schemes, as compared to Ref. [30], are explained by the usage of the static scale in the calculations. Switching to the $\overline{\text{MS}}$ or MSR mass scheme does not affect the scale uncertainties anymore. In the light of this observation, it will be worth to develop the transition to the other mass schemes in the MadGraph5_aMC@NLO program directly, such that predictions for differential $t\bar{t}$ cross sections in association with jets can be obtained in the format which is suitable for PDF fits in different mass schemes and with dynamic scales. Furthermore, we do not observe any noticeably larger theoretical uncertainty when using the $\overline{\text{MS}}$ running mass instead of the pole mass, as was reported in Refs. [18, 36]. Switching from the pole mass scheme to the MSR mass scheme with $R = 3$ GeV changes the extracted mass value by 0.3 GeV only which is well within the current experimental and theoretical uncertainties.

The extracted value of $m_t(m_t)$ is compared with several other determinations in Fig. 8. In the ABMP16 analysis, the running top quark mass was determined from measurements of total top quark pair and single top production cross sections in a global QCD fit at NNLO [37]. In Ref. [18] ATLAS extracted $m_t(m_t)$ at NLO from their measurement of $t\bar{t} + 1$ jet production cross sections. In Ref. [36] Fuster at al. extracted $m_t(m_t)$ at NLO using the Run-1 ATLAS measurement of $t\bar{t} + 1$ jet production [38]. Currently, the world average value of $m_t(m_t)$ [17] is based on a single determination of this parameter by the D0 collaboration at approximate NNLO [39]. When comparing to the other determinations of $m_t(m_t)$ displayed in Fig. 8, it is worthy of attention that only the results of this work and ABMP16 analysis are obtained in a simultaneous fit of $m_t(m_t)$, α_s and PDFs, while the other determinations were done using a given value of α_s and PDF set.

## 5.3 NNLO PDF fits with total charm hadroproduction cross section

The NLO predictions for differential charm hadroproduction at the LHC have very large ($> 100\%$ in some regions of the phase space) scale uncertainties. Furthermore most of the PDF fitting groups provide fits at NNLO accuracy. This prevents including existing data on charm and bottom hadroproduction in their state-of-the-art fits. In this context measurements of the total charm hadroproduction cross section would be beneficial, because they can be confronted in the fits with NNLO predictions [40–43] which have reduced scale uncertainties. However, no such measurements

Settings	Fit results
pole mass, $\mu_r = \mu_f = H'$, Ref. [30]	$\chi^2 = 1364$, $\chi^2_{t\bar{t}} = 20$ $m_t^{\text{pole}} = 170.5 \pm 0.7(\text{fit}) \pm 0.1(\text{mod})^{+0.0}_{-0.1}(\text{par}) \pm 0.3(\mu)$ GeV $\alpha_s = 0.1135 \pm 0.0016(\text{fit})^{+0.0002}_{-0.0004}(\text{mod})^{+0.0008}_{-0.0001}(\text{par})^{+0.0011}_{-0.0005}(\mu)$
pole mass, $\mu_r = \mu_f = m_t$, this work	$\chi^2 = 1363$, $\chi^2_{t\bar{t}} = 19$ $m_t^{\text{pole}} = 169.9 \pm 0.7(\text{fit}) \pm 0.1(\text{mod})^{+0.0}_{-0.0}(\text{par})^{+0.3}_{-0.9}(\mu)$ GeV $\alpha_s = 0.1132 \pm 0.0016(\text{fit})^{+0.0003}_{-0.0004}(\text{mod})^{+0.0003}_{-0.0000}(\text{par})^{+0.0016}_{-0.0008}(\mu)$
$\overline{\text{MS}}$ mass, $\mu_r = \mu_f = m_t$, this work	$\chi^2 = 1363$, $\chi^2_{t\bar{t}} = 19$ $m_t(m_t) = 161.0 \pm 0.6(\text{fit}) \pm 0.1(\text{mod})^{+0.0}_{-0.0}(\text{par})^{+0.4}_{-0.8}(\mu)$ GeV $\alpha_s = 0.1136 \pm 0.0016(\text{fit})^{+0.0002}_{-0.0005}(\text{mod})^{+0.0002}_{-0.0001}(\text{par})^{+0.0015}_{-0.0009}(\mu)$
MSR mass ($R = 3$ GeV), $\mu_r = \mu_f = m_t$, this work	$\chi^2 = 1363$, $\chi^2_{t\bar{t}} = 19$ $m_t^{\text{MSR}} = 169.6 \pm 0.7(\text{fit}) \pm 0.1(\text{mod})^{+0.0}_{-0.0}(\text{par})^{+0.3}_{-0.9}(\mu)$ GeV $\alpha_s = 0.1132 \pm 0.0016(\text{fit})^{+0.0003}_{-0.0004}(\text{mod})^{+0.0002}_{-0.0000}(\text{par})^{+0.0016}_{-0.0008}(\mu)$

Table 3. The values of top quark mass in different mass scheme and α_s obtained in Ref. [30] and this work in the fit to the CMS data on $t\bar{t}$ production and HERA DIS data. The fit, model (mod), parametrisation (par) and scale variation (μ) uncertainties are reported. Also the values of χ^2 are reported, as well as the partial χ^2 values for $t\bar{t}$ data ($\chi^2_{t\bar{t}}$) for 23 $t\bar{t}$ cross section bins in the fit.

have been performed to date. On the other hand, ALICE [44, 45], ATLAS [46] and LHCb [23, 47, 48] experiments provided measurements of charm production in different kinematic regions which cover more than one half of the phase space. One can reliably extract the total cross section by extrapolating these measurements to the full phase space. The extrapolation procedure is similar to extracting reduced cross sections for charm production at HERA [29] from measurements in a fiducial phase space, which are then used in global PDF fits. Below we perform such extrapolation, provide values for the total charm cross section at different center-of-mass energies and their ratios together with experimental and theoretical uncertainties arising from the extrapolation procedure, compare to theoretical predictions at NNLO which are obtained using different PDF sets, and demonstrate how these data can help reducing PDF uncertainties.

The existing most precise LHC measurements of charm production are summarised in Table 4. The ALICE measurements at 5 and 7 TeV cover the central region $|y| < 0.5$, the LHCb measurements at 5, 7 and 13 TeV provide coverage of the forward region $2 < y < 4.5$, and the ATLAS measurement at 7 TeV essentially bridges the gap by providing data at $|\eta| < 2.1$. However, while both ALICE and
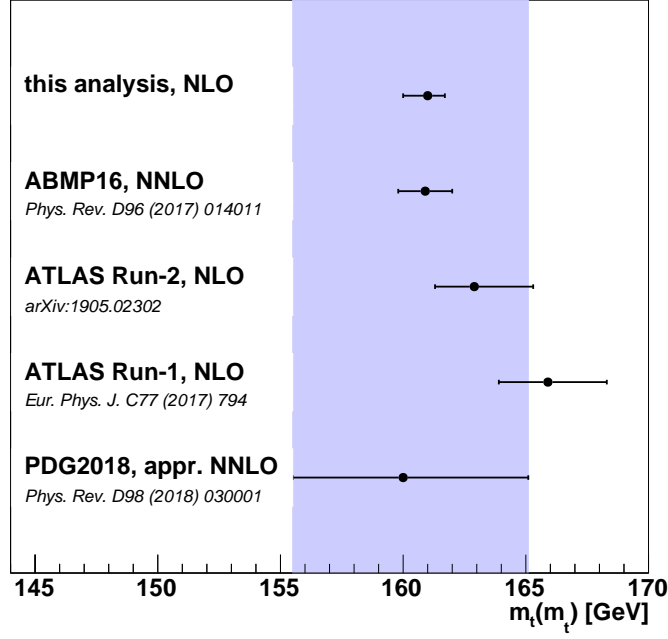
Figure 8. The extracted value of $m_t(m_t)$ compared to other determinations. 'ATLAS Run-1, NLO' refers to the extraction of $m_t(m_t)$ by Fuster et al. [36] using the Run-1 ATLAS measurement of $t\bar{t}+1$ jet production. The world average 'PDG2018, appr. NNLO' is based on a single determination of the D0 collaboration [39].

LHCb provide measurements nearly in the full p_T range starting from 0 GeV, AT-LAS reports the cross sections only at $p_T > 3.5$ GeV, thus leaving the bulk of the corresponding p_T kinematic range unmeasured. Furthermore, it turns out that the most precise data for ALICE and LHCb are available for D^0 production, while this final state was not measured by ATLAS. Given these arguments, at 5 and 7 TeV we extrapolate ALICE and LHCb measurements of D^0 production to the full phase space. In order to maintain least dependence on the theoretical predictions, both ALICE and LHCb measurements are extrapolated to nearby regions of y, namely to $0 < |y| < 1.5$ and $|y| > 1.5$, respectively:

$$\sigma_{\text{total}} = \sigma_{\text{ALICE}} \times K_{\text{ALICE}} + \sigma_{\text{LHCb}} \times K_{\text{LHCb}} \times 2$$

$$K_{\text{ALICE}} = \frac{\sigma^{NLO}_{|y|<1.5}}{\sigma^{\text{NLO}}_{|y|<0.5}}, \qquad K_{\text{LHCb}} = \frac{\sigma^{NLO}_{|y|>1.5}}{\sigma^{\text{NLO}}_{2<|y|<4.5}}. \tag{5.2}$$

Here σ_{ALICE} and σ_{LHCb} are the ALICE and LHCb data, respectively, and σ^{NLO} is the theoretical prediction. The factor 2 in the second term takes into account that the LHCb data are provided for only $2 < y < 4.5$ and need to be extrapolated to $2 < |y| < 4.5$ (we exploit the symmetry around $y = 0$ and take that the cross sections at $2 < y < 4.5$ and $-4.5 < y < -2$ are equal). Also the measurements are extrapolated into the full range of p_T (not shown in Eq. 5.2 for brevity), which

Measurement	Final state	Kinematic region
ALICE 5 TeV [45]	D^0, D^+, D^{*+}, D_s^+	$0 < p_T < 36$ GeV, $|y| < 0.5$
ALICE 7 TeV [45]	D^0, D^+, D^{*+}, D_s^+	$0 < p_T < 36$ GeV, $|y| < 0.5$
ATLAS 7 TeV [46]	D^+, D^{*+}, D_s^+	$3.5 < p_T < 100$ GeV, $|\eta| < 2.1$
LHCb 5 TeV [48]	D^0, D^+, D^{*+}, D_s^+	$0 < p_T < 10$ GeV, $2 < y < 4.5$
LHCb 7 TeV [23]	D^0, D^+, D^{*+}, D_s^+, Λ_c	$0 < p_T < 8$ GeV, $2 < y < 4.5$
LHCb 13 TeV [47]	D^0, D^+, D^{*+}, D_s^+	$0 < p_T < 15$ GeV, $2 < y < 4.5$

Table 4. Summary of most precise measurements of charm production at the LHC.

implies only 1% correction for the LHCb data at 7 TeV provided for $p_T < 8$ GeV, and even smaller corrections for the other data sets. This procedure is used to obtain the total cross section for D^0 production at 5 and 7 TeV, while at 13 TeV we extrapolate solely the LHCb measurement since no other data are available at this energy. We calculate the total charm production cross section from the D^0 production cross section dividing the latter by the fragmentation fraction from Ref. [49]:

$$\sigma(c\bar{c}) = \sigma(D^0)/(2f(c \to D^0)), \quad f(c \to D^0) = 0.6141 \pm 0.0073. \qquad (5.3)$$

The factor 2 in Eq. 5.3 accounts that both c and $\bar{c}$ fragment into charmed hadrons. The uncertainty on $f(c \to D^0)$ which amounts to 1% is neglected. We also compute ratios of cross sections at different centre-of-mass energies $R_{7/5} = \sigma_{7\ \text{TeV}}/\sigma_{5\ \text{TeV}}$ and $R_{13/7} = \sigma_{13\ \text{TeV}}/\sigma_{7\ \text{TeV}}$ which benefit from partial cancellation of theoretical uncertainties.

The theoretical prediction σ^{NLO} are computed using the NLO predictions with the $\overline{\text{MS}}$ masses described in the previous sections, supplemented with phenomenological non-pertutbative fragmentation functions to describe the $c \to D^0$ transition. The factorisation and renormalisation scales are chosen to be $\mu_r = \mu_f = \sqrt{4m_c(m_c)^2 + p_T^2}$ and varied by a factor of two up and down (both simultaneously and independently for μ_r and μ_f) to estimate the uncertainties. The $\overline{\text{MS}}$ charm quark mass is set to $m_c(m_c) = 1.275 \pm 0.030$ GeV [17]. The proton is described by the PROSA PDF set [20]. We chose this set because among all FFNS PDF sets which are available today the PROSA set is expected to have the most reliable gluon distribution at low x thanks to the heavy-quark data used for its determination. Furthermore, to estimate the PDF uncertainties, the extrapolation is performed using the ABMP16 [19], CT14 [50], MMHT2014 [51], JR14 [52], NNPDF3.1 [53] and HERAPDF FF3A [35] NLO PDF sets, and the envelope covering the PROSA PDF uncertainties and the difference obtained using any of the additional PDF sets is constructed. This conservative procedure is essential, because the theoretical calculations for highest values of y involve the gluon PDF at very low values of x (up to 4×10^{-8}) where it is

not directly covered by data in any of the PDF fits (even in the PROSA fit which includes the charm data up to $y = 4.5$ as measured by LHCb). The fragmentation of charm quarks into D^0 mesons is described by the Kartvelishvili function with $\alpha_K = 4.4 \pm 1.7$ [20], while the fragmentation fraction $f(c \to D^0)$ cancels for the extrapolation factors in Eq. 5.2. All theoretical uncertainties are assumed to be fully correlated for cross sections in different kinematic regions and at different centre-of-mass energies. Robustness of the extrapolation procedure is checked by varying the boundary y between the kinematic regions into which the ALICE and LHCb measurements are extrapolated by ± 0.5 (at the same time, this variation tests consistency of the ALICE and LHCb data). Furthermore, we did another check of the extrapolation procedure by computing predictions for the ALICE and LHCb data using the POWHEGBOX + PYTHIA6 framework which provide NLO predictions matched to parton showers and found them to be consistent with our NLO calculations within the theoretical uncertainties.

The results of extrapolation are reported in Table 5. The scale, mass, PDF and fragmentation uncertainties are added in quadrature to obtain the total theoretical uncertainty assigned to the extrapolated results. The experimental uncertainties of the input data are propagated to the extrapolated cross sections and reported separately. The experimental uncertainties of the input data sets are assumed to be fully uncorrelated. The experimental and theoretical extrapolation uncertainties are of the same size. The total uncertainties are obtained by adding the experimental and theoretical uncertainties in quadrature, and amount to $\approx 10\%$. Our value for the total charm cross section at 7 TeV is in agreement with the extrapolated cross sections reported in Refs. [45, 46, 54] within uncertainties.

The extrapolated cross sections and their ratios are compared to NNLO predictions obtained using different PDF sets. Namely, we used the ABMP16 [37], CT14 [50], MMHT2014 [51], JR14 [52], NNPDF3.1 [53] and HERAPDF [35] NNLO PDF sets. The cross sections are computed using the HATHOR program [55] interfaced in xFitter [15]. The factorisation and renormalisation scales are chosen to be $\mu_r = \mu_f = 2m_c(m_c)$ and varied by a factor of two up and down (both simultaneously and independently for μ_r and μ_f) to estimate the uncertainties. The $\overline{\text{MS}}$ charm quark mass is set to $m_c(m_c) = 1.275$ GeV [17]. Figure 9 shows the extrapolated cross sections and their ratios compared to NNLO predictions. For the NNLO predictions, separately the theoretical uncertainty which arise from the scale variations and the PDF uncertainty is shown. All theoretical predictions agree with the data within uncertainties, but noticeably the MMHT2014, HERAPDF2.0 and CT14 PDF sets have uncertainties which are larger than both scale and data extrapolation uncertainties for some of the observables. In particular, for the cross sections at 13 TeV the predictions of the MMHT2014 and HERAPDF2.0 sets are consistent with negative values within uncertainties, while the CT14 predictions has a large positive uncertainty which greatly exceeds our extrapolated cross section. Therefore, these

PDF sets could benefit from data on charm production cross sections or their ratios included in the fits. Remarkably, also the scale uncertainties appear to be different when using different PDF sets. Among the considered observables, the most conclusive one is $R_{7/5}$ for which both data extrapolation and theoretical scale uncertainties are moderate ($\approx 10\%$). Our extrapolated value for this observable can be used in future NNLO PDF fits to constrain the gluon PDF at low x. The other ratio $R_{13/7}$ has a larger extrapolation uncertainty suffering from the lack of experimental measurements of charm production in the central rapidity region at 13 TeV.

Observable \Unc. [%]	NLO μ var.	$m_c(m_c) \pm 0.03$ GeV	$\alpha_K \pm 1.7$	PDF	$y_{\text{ALICE,LHCb}} \pm 0.5$	Total th.	Exp.	Total
$\sigma(c\bar{c})_{5\text{TeV}}/\text{mb} = 5.254$	$^{+0.8}_{-0.6}$	$^{-0.1}_{+0.1}$	$^{-2.0}_{+1.1}$	$^{+4.8}_{-1.5}$	$^{-2.0}_{+2.2}$	$^{+5.0}_{-2.5}$	± 4.3	$^{+6.6}_{-5.0}$
$\sigma(c\bar{c})_{7\text{TeV}}/\text{mb} = 6.311$	$^{+0.7}_{-0.6}$	$^{-0.1}_{+0.1}$	$^{-2.0}_{+1.1}$	$^{+7.8}_{-1.9}$	$^{-2.2}_{+2.4}$	$^{+7.9}_{-2.8}$	± 6.5	$^{+10.2}_{-7.1}$
$\sigma(c\bar{c})_{13\text{TeV}}/\text{mb} = 11.298$	$^{+0.7}_{-2.9}$	$^{+0.2}_{-0.2}$	$^{+1.5}_{-0.6}$	$^{+0.0}_{-2.9}$	n/a	$^{+1.6}_{-4.1}$	± 6.1	$^{+6.3}_{-7.3}$
$R_{7/5} = 1.201$	$^{+0.1}_{-0.0}$	$^{+0.0}_{-0.0}$	$^{-0.0}_{+0.0}$	$^{+2.9}_{-0.4}$	n/a	$^{+2.9}_{-0.4}$	± 7.8	$^{+8.3}_{-7.8}$
$R_{13/7} = 1.790$	$^{+1.3}_{-3.5}$	$^{+0.2}_{-0.2}$	$^{+3.6}_{-1.7}$	$^{+1.0}_{-8.5}$	n/a	$^{+3.9}_{-9.3}$	± 8.9	$^{+9.7}_{-12.9}$

Table 5. Extrapolated total charm production cross sections and their ratios at different centre-of-mass energies. The correlation factor between $R_{7/5}$ and $R_{13/7}$ is -0.61.

To demonstrate the feasibility of the provided observables to constrain the PDFs, we employ a profiling technique [56] based on minimizing χ^2 function between data and theoretical predictions taking into account both data and theoretical uncertainties arising from PDF variations. The analysis is performed using the xFitter program [15]. We consider the MMHT2014 PDF set and the ratios $R_{7/5}$ and $R_{13/7}$ which exhibit least scale uncertainties. The correlation of $R_{7/5}$ and $R_{13/7}$ because of the common input 7 TeV data sets is taken into account. The PDF uncertainties are included in χ^2 through nuisance parameters, and the values of these nuisance parameters at the minimum are interpreted as optimised (or profiled) PDFs, while their uncertainties determined using the tolerance criterion of $\Delta\chi^2 = 1$ correspond to the new PDF uncertainties. The original and profiled MMHT2014 gluon PDF is shown in Fig. 10 at the scale $Q^2 = 10$ and 100 GeV^2. The profiled distribution exhibits greatly reduced uncertainties at low x, and in this region the distribution is shifted towards larger values of the gluon density.

5.4 Prompt neutrino fluxes

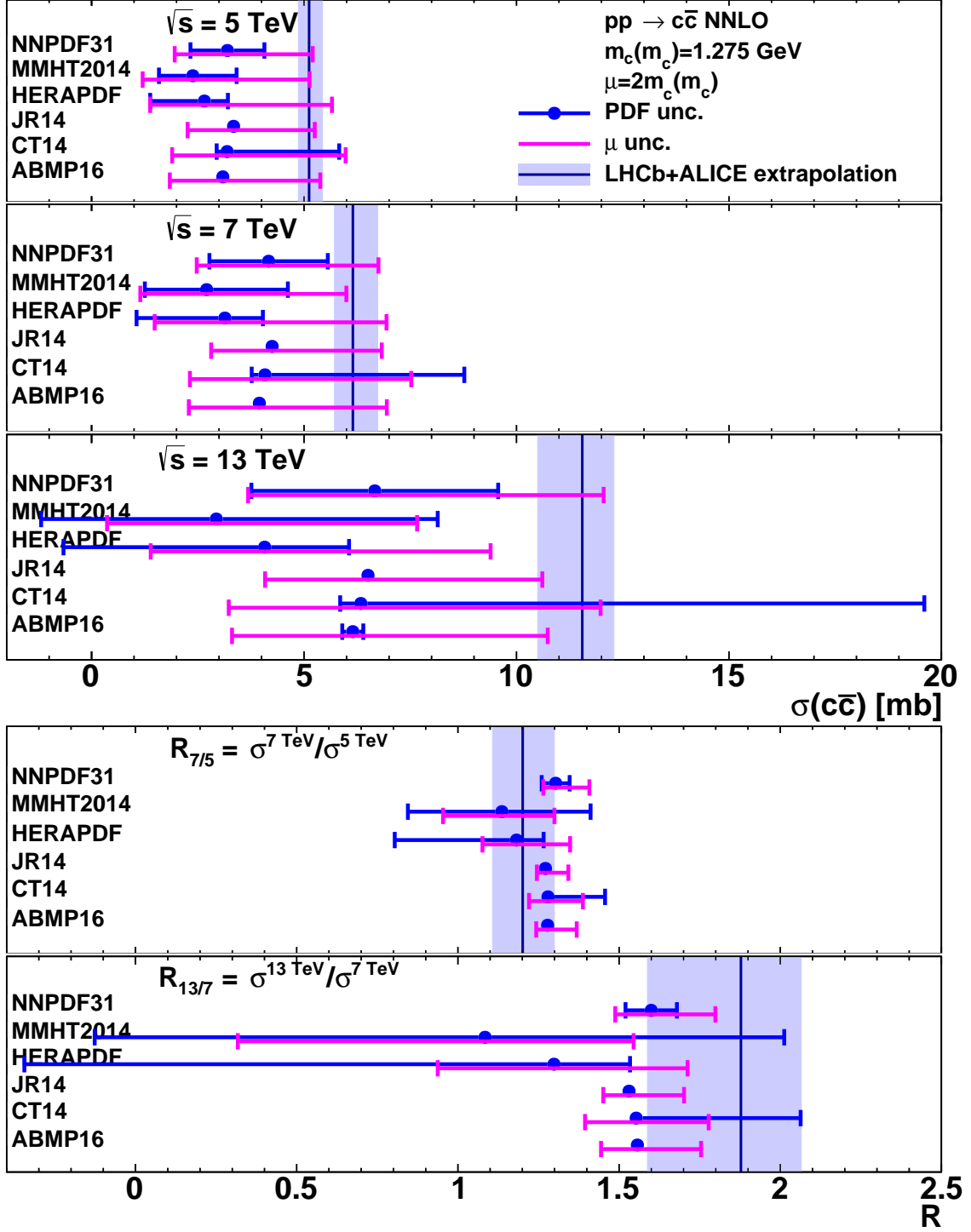....Discussion at qualitative level about reduction of uncertainties.
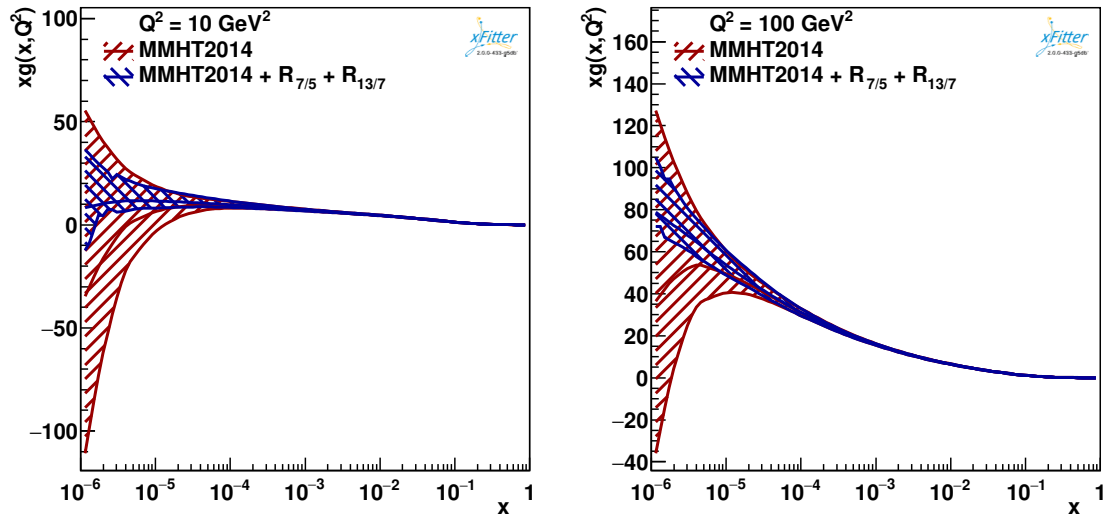
6 Conclusions

Appendix: description of the routines added to MCFM

...name of routines, what they do, how to compile....

Figure 9. Comparison of the extrapolated total charm production cross sections and their ratios with the NNLO theoretical predictions using different PDF sets.

Figure 10. The gluon distribution of the original and profiled MMHT2014 set at $Q^2 = 10$ GeV^2 (left) and $Q^2 = 100$ GeV^2 (right).

References

[1] M. Beneke, *A Quark mass definition adequate for threshold problems*, *Phys. Lett.* **B434** (1998) 115–125, [`hep-ph/9804241`].

[2] A. H. Hoang and T. Teubner, *Top quark pair production close to threshold: Top mass, width and momentum distribution*, *Phys. Rev.* **D60** (1999) 114027, [`hep-ph/9904468`].

[3] S. Fleming, A. H. Hoang, S. Mantry, and I. W. Stewart, *Jets from massive unstable particles: Top-mass determination*, *Phys. Rev.* **D77** (2008) 074010, [`hep-ph/0703207`].

[4] K. G. Chetyrkin and M. Steinhauser, *Short distance mass of a heavy quark at order* α_s^3, *Phys. Rev. Lett.* **83** (1999) 4001–4004, [`hep-ph/9907509`].

[5] P. Marquard, A. V. Smirnov, V. A. Smirnov, and M. Steinhauser, *Quark Mass Relations to Four-Loop Order in Perturbative QCD*, *Phys. Rev. Lett.* **114** (2015), no. 14 142002, [`arXiv:1502.01030`].

[6] S. Moch et al., *High precision fundamental constants at the TeV scale*, `arXiv:1405.4781`.

[7] N. Gray, D. J. Broadhurst, W. Grafe, and K. Schilcher, *Three Loop Relation of Quark (Modified) Ms and Pole Masses*, *Z. Phys.* **C48** (1990) 673–680.

[8] K. G. Chetyrkin and M. Steinhauser, *The Relation between the MS-bar and the on-shell quark mass at order alpha(s)**3*, *Nucl. Phys.* **B573** (2000) 617–651, [`hep-ph/9911434`].

[9] K. Melnikov and T. v. Ritbergen, *The Three loop relation between the MS-bar and the pole quark masses*, *Phys. Lett.* **B482** (2000) 99–108, [`hep-ph/9912391`].

[10] A. H. Hoang, A. Jain, I. Scimemi, and I. W. Stewart, *Infrared Renormalization Group Flow for Heavy Quark Masses*, *Phys. Rev. Lett.* **101** (2008) 151602, [`arXiv:0803.4214`].

[11] B. Schmidt and M. Steinhauser, *CRunDec: a C++ package for running and decoupling of the strong coupling and quark masses*, *Comput. Phys. Commun.* **183** (2012) 1845–1848, [`arXiv:1201.6149`].

[12] J. M. Campbell and R. K. Ellis, *An Update on vector boson pair production at hadron colliders*, *Phys. Rev.* **D60** (1999) 113006, [`hep-ph/9905386`].

[13] J. M. Campbell, R. K. Ellis, and C. Williams, *Vector boson pair production at the LHC*, *JHEP* **07** (2011) 018, [`arXiv:1105.0020`].

[14] M. Dowling and S.-O. Moch, *Differential distributions for top-quark hadro-production with a running mass*, *Eur. Phys. J.* **C74** (2014), no. 11 3167, [`arXiv:1305.6422`].

[15] S. Alekhin et al., *HERAFitter*, *Eur. Phys. J.* **C75** (2015), no. 7 304, [`arXiv:1410.4412`].

[16] M. L. Mangano, P. Nason, and G. Ridolfi, *Heavy quark correlations in hadron collisions at next-to-leading order*, *Nucl. Phys.* **B373** (1992) 295–345.

[17] **Particle Data Group** Collaboration, M. Tanabashi et al., *Review of Particle Physics*, *Phys. Rev.* **D98** (2018), no. 3 030001.

[18] **ATLAS** Collaboration, G. Aad et al., *Measurement of the top-quark mass in $t\bar{t} + 1$-jet events collected with the ATLAS detector in pp collisions at $\sqrt{s} = 8$ TeV*, arXiv:1905.02302.

[19] S. Alekhin, J. Bl"umlein, and S. Moch, *NLO PDFs from the ABMP16 fit*, *Eur. Phys. J.* **C78** (2018), no. 6 477, [arXiv:1803.07537].

[20] **PROSA** Collaboration, O. Zenaiev et al., *Impact of heavy-flavour production cross sections measured by the LHCb experiment on parton distribution functions at low x*, *Eur. Phys. J.* **C75** (2015), no. 8 396, [arXiv:1503.04581].

[21] R. Gauld, J. Rojo, L. Rottoli, and J. Talbert, *Charm production in the forward region: constraints on the small-x gluon and backgrounds for neutrino astronomy*, *JHEP* **11** (2015) 009, [arXiv:1506.08025].

[22] R. Gauld and J. Rojo, *Precision determination of the small-x gluon from charm production at LHCb*, *Phys. Rev. Lett.* **118** (2017), no. 7 072001, [arXiv:1610.09373].

[23] **LHCb** Collaboration, R. Aaij et al., *Prompt charm production in pp collisions at sqrt(s)=7 TeV*, *Nucl. Phys.* **B871** (2013) 1–20, [arXiv:1302.2864].

[24] **LHCb** Collaboration, R. Aaij et al., *Measurement of B meson production cross-sections in proton-proton collisions at $\sqrt{s} = 7$ TeV*, *JHEP* **08** (2013) 117, [arXiv:1306.3663].

[25] **H1, ZEUS** Collaboration, F. D. Aaron et al., *Combined Measurement and QCD Analysis of the Inclusive e+- p Scattering Cross Sections at HERA*, *JHEP* **01** (2010) 109, [arXiv:0911.0884].

[26] **H1, ZEUS** Collaboration, H. Abramowicz et al., *Combination and QCD Analysis of Charm Production Cross Section Measurements in Deep-Inelastic ep Scattering at HERA*, *Eur. Phys. J.* **C73** (2013), no. 2 2311, [arXiv:1211.1182].

[27] **ZEUS** Collaboration, H. Abramowicz et al., *Measurement of beauty and charm production in deep inelastic scattering at HERA and measurement of the beauty-quark mass*, *JHEP* **09** (2014) 127, [arXiv:1405.6915].

[28] **xFitter Developers' Team** Collaboration, V. Bertone et al., *A determination of $m_c(m_c)$ from HERA data using a matched heavy-flavor scheme*, *JHEP* **08** (2016) 050, [arXiv:1605.01946].

[29] **H1, ZEUS** Collaboration, H. Abramowicz et al., *Combination and QCD analysis of charm and beauty production cross-section measurements in deep inelastic ep scattering at HERA*, *Eur. Phys. J.* **C78** (2018), no. 6 473, [arXiv:1804.01019].

[30] **CMS** Collaboration, A. M. Sirunyan et al., *Measurement of $t\bar{t}$ normalised multi-differential cross sections in pp collisions at $\sqrt{s} = 13$ TeV, and simultaneous

determination of the strong coupling strength, top quark pole mass, and parton distribution functions, Submitted to: Eur. Phys. J. (2019) [arXiv:1904.05237].

[31] S. Alioli, P. Fernandez, J. Fuster, A. Irles, S.-O. Moch, P. Uwer, and M. Vos, *A new observable to measure the top-quark mass at hadron colliders*, Eur. Phys. J. **C73** (2013) 2438, [arXiv:1303.6415].

[32] J. Alwall, R. Frederix, S. Frixione, V. Hirschi, F. Maltoni, O. Mattelaer, H. S. Shao, T. Stelzer, P. Torrielli, and M. Zaro, *The automated computation of tree-level and next-to-leading order differential cross sections, and their matching to parton shower simulations*, JHEP **07** (2014) 079, [arXiv:1405.0301].

[33] V. Bertone, R. Frederix, S. Frixione, J. Rojo, and M. Sutton, *aMCfast: automation of fast NLO computations for PDF fits*, JHEP **08** (2014) 166, [arXiv:1406.7693].

[34] T. Carli, D. Clements, A. Cooper-Sarkar, C. Gwenlan, G. P. Salam, F. Siegert, P. Starovoitov, and M. Sutton, *A posteriori inclusion of parton density functions in NLO QCD final-state calculations at hadron colliders: The ApplGrid project*, Eur. Phys. J. C **66** (2010) 503, [arXiv:0911.2985].

[35] **H1, ZEUS** Collaboration, H. Abramowicz et al., *Combination of measurements of inclusive deep inelastic $e^{\pm}p$ scattering cross sections and QCD analysis of HERA data*, Eur. Phys. J. **C75** (2015), no. 12 580, [arXiv:1506.06042].

[36] J. Fuster, A. Irles, D. Melini, P. Uwer, and M. Vos, *Extracting the top-quark running mass using $t\bar{t}$ + 1-jet events produced at the Large Hadron Collider*, Eur. Phys. J. **C77** (2017), no. 11 794, [arXiv:1704.00540].

[37] S. Alekhin, J. Bl"umlein, S. Moch, and R. Placakyte, *Parton distribution functions, α_s, and heavy-quark masses for LHC Run II*, Phys. Rev. **D96** (2017), no. 1 014011, [arXiv:1701.05838].

[38] **ATLAS** Collaboration, G. Aad et al., *Determination of the top-quark pole mass using $t\bar{t}$ + 1-jet events collected with the ATLAS experiment in 7 TeV pp collisions*, JHEP **10** (2015) 121, [arXiv:1507.01769].

[39] **D0** Collaboration, V. M. Abazov et al., *Determination of the pole and $\overline{MS}$ masses of the top quark from the $t\bar{t}$ cross section*, Phys. Lett. **B703** (2011) 422–427, [arXiv:1104.2887].

[40] P. Bärnreuther, M. Czakon, and A. Mitov, *Percent Level Precision Physics at the Tevatron: First Genuine NNLO QCD Corrections to $q\bar{q} \to t\bar{t} + X$*, Phys. Rev. Lett. **109** (2012) 132001, [arXiv:1204.5201].

[41] M. Czakon and A. Mitov, *NNLO corrections to top-pair production at hadron colliders: the all-fermionic scattering channels*, JHEP **12** (2012) 054, [arXiv:1207.0236].

[42] M. Czakon and A. Mitov, *NNLO corrections to top pair production at hadron colliders: the quark-gluon reaction*, JHEP **01** (2013) 080, [arXiv:1210.6832].

[43] M. Czakon, P. Fiedler, and A. Mitov, *Total Top-Quark Pair-Production Cross Section at Hadron Colliders Through $O(\alpha\frac{4}{S})$*, Phys. Rev. Lett. **110** (2013) 252004, [arXiv:1303.6254].

[44] **ALICE** Collaboration, S. Acharya et al., *Measurement of D-meson production at mid-rapidity in pp collisions at $\sqrt{s} = 7$ TeV*, Eur. Phys. J. **C77** (2017), no. 8 550, [arXiv:1702.00766].

[45] **ALICE** Collaboration, S. Acharya et al., *Measurement of D^0 , D^+ , D^{*+} and D_s^+ production in pp collisions at $\sqrt{s} = 5.02$ TeV with ALICE*, Eur. Phys. J. **C79** (2019), no. 5 388, [arXiv:1901.07979].

[46] **ATLAS** Collaboration, G. Aad et al., *Measurement of $D^{*\pm}$, $D^{\pm}$ and $D_s^{\pm}$ meson production cross sections in pp collisions at $\sqrt{s} = 7$ TeV with the ATLAS detector*, Nucl. Phys. **B907** (2016) 717–763, [arXiv:1512.02913].

[47] **LHCb** Collaboration, R. Aaij et al., *Measurements of prompt charm production cross-sections in pp collisions at $\sqrt{s} = 13$ TeV*, JHEP **03** (2016) 159, [arXiv:1510.01707]. [Erratum: JHEP05,074(2017)].

[48] **LHCb** Collaboration, R. Aaij et al., *Measurements of prompt charm production cross-sections in pp collisions at $\sqrt{s} = 5$ TeV*, JHEP **06** (2017) 147, [arXiv:1610.02230].

[49] M. Lisovyi, A. Verbytskyi, and O. Zenaiev, *Combined analysis of charm-quark fragmentation-fraction measurements*, Eur. Phys. J. **C76** (2016), no. 7 397, [arXiv:1509.01061].

[50] S. Dulat, T.-J. Hou, J. Gao, M. Guzzi, J. Huston, P. Nadolsky, J. Pumplin, C. Schmidt, D. Stump, and C. P. Yuan, *New parton distribution functions from a global analysis of quantum chromodynamics*, Phys. Rev. **D93** (2016), no. 3 033006, [arXiv:1506.07443].

[51] L. A. Harland-Lang, A. D. Martin, P. Motylinski, and R. S. Thorne, *Parton distributions in the LHC era: MMHT 2014 PDFs*, Eur. Phys. J. **C75** (2015), no. 5 204, [arXiv:1412.3989].

[52] P. Jimenez-Delgado and E. Reya, *Delineating parton distributions and the strong coupling*, Phys. Rev. **D89** (2014), no. 7 074049, [arXiv:1403.1852].

[53] **NNPDF** Collaboration, R. D. Ball et al., *Parton distributions from high-precision collider data*, Eur. Phys. J. **C77** (2017), no. 10 663, [arXiv:1706.00428].

[54] A. Bhattacharya, R. Enberg, M. H. Reno, I. Sarcevic, and A. Stasto, *Perturbative charm production and the prompt atmospheric neutrino flux in light of RHIC and LHC*, JHEP **06** (2015) 110, [arXiv:1502.01076].

[55] M. Aliev, H. Lacker, U. Langenfeld, S. Moch, P. Uwer, and M. Wiedermann, *HATHOR: HAdronic Top and Heavy quarks crOss section calculatoR*, Comput. Phys. Commun. **182** (2011) 1034–1046, [arXiv:1007.1327].

[56] H. Paukkunen and P. Zurita, *PDF reweighting in the Hessian matrix approach*, *JHEP* **12** (2014) 100, [arXiv:1402.6623].